Flavin-Mediated Reductive Deiodination: Conformational Events and Reactivity Pattern in the Active Site of Human Iodotyrosine Deiodinase

Soumyajit Karmakar and Sabyashachi Mishra*

Department of Chemistry, Indian Institute of Technology Kharagpur, Kharagpur, India

E-mail: mishra@chem.iitkgp.ac.in
Phone: +91-3222-282328

Abstract

Human iodotyrosine deiodinase (hIYD) catalyzes the reductive deiodination of iodotyrosine using a flavin mononucleotide cofactor to maintain iodine concentration in the body. Mutations in the hIYD gene are linked to human hypothyroidism, emphasizing its role in thyroid function regulation. The present work employs microsecond-scale molecular dynamics simulations and quantum chemical calculations to elucidate the conformational dynamics and reactivity in the active site at various stages of hIYD catalysis. The flavin is found to employ a unique butterfly motion of its isoalloxazine ring accompanied by a novel active-and-resting state of its ribose 2′-OH group during the catalytic cycle. The flavin dynamics is found to control substrate binding affinity, the active site lid closure, and NADPH recognition. The enzyme uses a group of basic residues (R100, R101, R104, K182, and R279) to stabilize flavin at different stages of catalysis, suggesting potential mutations to control enzyme activity. The reactivity descriptor analysis and stereo-electronic analysis predict the N5 nitrogen of flavin as a proton source during the reductive deiodination. The present findings provide key insights into the molecular basis of hIYD activity and lay the groundwork for future research aimed at therapeutic interventions and industrial applications.

Introduction

Iodine plays a crucial role in signaling pathways in the human thyroid gland.[1–6] During thyroid hormone biosynthesis, the breakdown of thyroglobulin produces 6-7 fold more iodinated tyrosines than thyroid hormones.[7,8] The loss of these iodinated tyrosines (I-Tyr) from the body can create a scarcity in the iodine pool of the thyroid gland.[8] Organisms have developed different mechanisms for dehalogenation of I-Tyr to maintain this iodine pool.[9,10] While anaerobes employ reductive deiodination assisted by metal-containing cofactors, the use of hydrolytic or oxidative pathways for dehalogenation is more common in aerobic organisms.[9,10] In humans, two enzymes of thyroid gland can promote reductive deiodination reactions following two distinct pathways: Iodothyronine deiodinase (ID) uses a selenocysteine based strategy to promote reductive deiodination during thyroid hormone synthesis, and iodotyrosine deiodinase (IYD) uses a flavin mononucleotide (FMN) cofactor to promote the same reaction to deiodinase the mono- and diiodotyrosines (I-Tyr and I_2-Tyr) to maintain iodine pool of the body.[11–13] Human IYD (hIYD) is a promising target for different medicinal and industrial applications. Genetics and mutation studies show that hIYD gene mutations cause hypothyroidism in humans.[14,15] A novel halophenol dehalogenase, an enzyme designed from IYD, has been shown to scavenge toxic halogenated pollutants from the environment.[16]

The overall enzymatic cycle of hIYD can be segmented into four steps: (a) reductive dehalogenation of I-Tyr, (b) Tyr release from the active site, (c) NADPH-mediated flavin reduction, and (d) I-Tyr binding for subsequent catalysis (Figure 1). In the reductive deiodination step, I-Tyr is reduced to Tyr, and the flavin cofactor in hydroquinone form (FMN_{hq}) is oxidized to FMN_{ox} via two one-electron transfer steps.[11] The K_M and k_{cat} values of the deiodination step are found to be 19 μM and 0.12 s^{-1}, respectively.[10] Rapid kinetic study of dehalogenation established that for I-Tyr reduction, the initial proton transfer and/or first electron transfer controls the rate of deiodination reaction.[9] However, the source of the proton has remained unknown.[10,11] In a recent study, the steady-state concentration of the electrophilic species generated from I-Tyr is found to be crucial for reductive dehalogenation by hIYD.[10] The failure of hIYD to dehalogenate F-Tyr suggests the presence of a single-electron reduced neutral semiquinone state of flavin (FMN_{sq}) during catalysis.[9,11]

After the catalytic deiodination, the end product Tyr leaves the active site with a dissociation constant (K_D) $> 10^3$ μM.[11] The crystal structures of hIYD in the presence and absence of I-Tyr (PDB IDs: 4TTC and 4TTB, respectively) are superimposable with a root mean

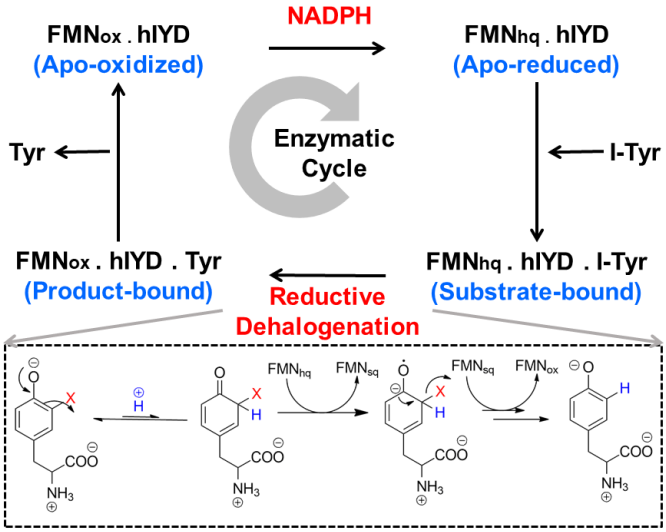

Figure 1: The overall enzymatic cycle of human IYD. The four steps involve (a) the reductive dehalogenation of I-Tyr, (b) Tyr release from the active site, (c) The NADPH-mediated flavin reduction, and (d) I-Tyr binding for the next catalytic cycle. The plausible catalytic mechanism of reductive deiodination is given in the box.

squared deviation (RMSD) of 0.47 Å.[11] However, the crystal structure in the absence of I-Tyr could not capture the electron density of the active site lid helix ($\alpha 5$) and the connected loops.[11] In this stage, where FMN_{ox} remians bound to the active site in the absence of Tyr, flavin undergoes an NADPH-mediated reduction to form FMN_{hq}. Previous studies showed that microsomal hIYD was responsive to the reduction by NADPH.[11] Surprisingly, the soluble hIYD, obtained as the crystal is not sensitive to NADPH.[17] Studies on BluB enzyme (from nitroreductase/flavin oxidoreductase family with 16 % structural similarity to hIYD) showed that the enzyme has an unusually tight binding pocket that can not accommodate NADPH with flavin,[18] further raising question on the mechanism of flavin reduction. After the NADPH-mediated reduction of flavin in the thyroid gland, a new I-Tyr binds the active site, in phenolate form,[11] with $K_D = 0.15$ μM and k_{on} 1.9×10^6 $M^{-1}s^{-1}$.[9]

While the previous studies have shed light on the binding kinetics and mechanistic pathway of the unusual dehalogenation reaction by hIYD, a molecular-level understanding of the factors controlling the binding constants of different substrates and the effect of conformational dynamics of the enzyme on the catalytic process is missing. Human IYD is a vital enzyme for its contribution to human health. Understanding the conformational dynamics of the enzyme and its role in I-Tyr/Tyr association with flavin in the active site will be very insightful for future enzyme design efforts. The role of the dynamic nature of the important active site residues in catalysis is also crucial for identifying fatal mutations of the enzyme that can cause hypothyroidism. In the present study, we provide an account of the conformational dynamics of hIYD through all-atom molecular dynamics (MD) simulations. We compare the four thermodynamic equilibrium states of the enzymatic cycle (Figure 1) to identify critical factors regulating each step. Our simulations characterise the butterfly movement of flavin at different stages of catalysis, estimate the binding affinity of ligands in the changing active site environments, and identify the key residues in stabilizing the ligands. We use local reactivity descriptors to identify the reactive centres of flavin inside the protein matrix and obtain a structural model consistent with NADPH-mediated flavin reduction. The reactivity descriptor analysis combined with stereoelectronic analysis shows that N5 nitrogen of flavin can act as a proton source during reductive deiodination.

Computational Methods

The X-ray crystal structure of hIYD complexed with FMN_{hq} and I-Tyr (PDB ID: 4TTC)[11] was used as the starting structure to build four models, each representing a thermodynamic state of the four steps of the enzymatic cycle, namely, FMN_{ox}·hIYD, FMN_{hq}·hIYD, FMN_{hq}·hIYD·I−Tyr, and FMN_{ox}·hIYD·Tyr states (Figure 1). All protonation states were assigned using H++ server,[19] and the ff14SB force-field[20] was used for all amino acids. Sodium and chloride ions were added as counter ions to neu-

tralize the systems and to maintain a salt concentration of 150 mM. For each model, the partial charges of FMN (FMN_{hq} and FMN_{ox}) and I-Try/Tyr were obtained using RESP method[21] from the electron density obtained with B3LYP+D3/def2tzvp method (Tables S1, S2, S3). The other force field parameters of the ligands were taken from the General Amber Force Field (GAFF)[22] (details in the supporting information). I-Tyr and Tyr were modeled in phenolate form.[11] The enzyme-ligand complex was enclosed in a water box together with periodic boundary conditions. Water molecules were treated with TIP3P model.[23] The system was prepared with AmberTools18 and simulations were run with AMBER18 package.[24] An initial heating simulation was run for 1 ns, with constant N and V, up to a desired temperature of 300 K, followed by a 12 ns stepwise equilibration in the NVT ensemble. An integration time step of 1 fs was used using SHAKE algorithm[25] to constrain all hydrogen-containing covalent bonds, and a non-bonded cut-off of 10 Å was used to define explicit particle-particle electrostatic interactions. Electrostatic interactions beyond 8 Å were treated with a particle-mesh Ewald (PME) summation method.[26] For temperature scaling, the Langevin thermostat[27] with a collision frequency of 5 ps^{-1} was used. The equilibration of each model was verified using the backbone root mean square deviation (RMSD) of the enzyme (Figure S4). After equilibration, a 1 μs classical molecular dynamics (MD) simulation was run for each model in an NTP ensemble with an integration time step of 2 fs, at 1 bar and 300 K, with a Berendsen barostat[28] with isotropic position scaling and pressure relaxation time of 1 ps. The MD trajectories were analyzed using cpptraj module[29] and in-house Python codes. Further details of the MD simulation are given in the supporting information.

Molecular mechanics Poisson Boltzmann surface area (MM-PBSA) method[30] was employed to determine the binding free energy of ligands (I-Tyr/Tyr) and cofactors (FMN_{hq} /FMN_{ox}) in different stages of hIYD catalysis. The binding energy for FMN_{hq}, FMN_{ox}, I-Tyr, and Tyr were estimated from the MM-PBSA calculations carried out on 10 short trajectories (each 10 ns long) that were started from the last snapshot of the 1 μs trajectories of FMN_{hq}·hIYD·I−Tyr, FMN_{ox}·hIYD·Tyr, FMN_{ox}·hIYD, and FMN_{hq}·hIYD systems, respectively. The total MM-PBSA free energy was further decomposed residue-wise. The entropy contribution to the free energy was neglected since the binding free energy is compared between ligands of similar size binding to the same protein, and secondly, the entropy calculated from quasi-harmonic normal mode analysis tends to have a large margin of error that introduces significant uncertainty in the result.[30,31] Further details of the MM-PBSA calculation are given in the supporting information.

Quantum chemical calculations on model systems representing various stages of enzyme catalysis are performed to predict the trends in reactivity. To that end, we modeled six model systems, i.e., (a) isolated FMN_{hq}, (b) FMN_{hq} in presence of T239 and R104 residues interacting with isoalloxazine ring of flavin, (c) FMN_{hq} in presence of I-Tyr in phenolate form, (d) model (c) with T238, R104, and A130B interacting with isoalloxazine ring of flavin and I-Tyr, and (e and f) model (c) and (d), respectively, but with I-Tyr in phenol form. In all cases, FMN_{hq} was modeled as isoalloxazine ring up to 2′-OH group. For T238, T239, and R104, only the side chains were taken in QM calculations. For A130B, the main chain (with the N-terminal capped with an acetyl group, and the C-terminal capped with a methyl group) was considered during QM calculations. The models were prepared from the equilibrated snapshots of the 1 μs MD trajectory of the FMN_{hq}·hIYD and FMN_{hq}·hIYD·I−Tyr systems. The model systems, with the number of atoms varying between 37 to 103, were treated with DFT-B3LYP(D3)/def2tzvp using Gaussian 16 program.[32] The resulting wave functions were used for further analysis, including the frontier molecular orbitals (HOMO and LUMO), the Natural bonding orbitals (NBO), and the local reactivity descriptors (Fukui functions, further details are given in the ESI) using

Multiwfn3.8.[33]

Results and Discussion

Conformational dynamics in the overall enzymatic pathway

The flavoenzyme hIYD has three domains: an N-terminal trans-membrane domain, an intermediate domain, and a catalytic domain.[11] The native enzyme belongs to the NADH oxidase/flavin reductase superfamily and is a homo-dimer with 290 amino acids per monomer. However, the crystal structure (PDB ID: 4TTC) lacks the electron density of the N-terminal membrane region (residue 1-31), and a part of the intermediate domain (residue 32-70).[11] Each monomer hosts eight α helices, eight β strands, and six characteristic loops. The enzyme forms a domain-swapped dimer where α7 helices of each monomer form the dimer interface. FMN binds the dimer interface non-covalently (Figure 2(a)). Interactions of FMN with the enzyme environment can be segmented into three parts: (a) the salt-bridge interactions of the phosphate group of FMN with R100 and R101 making a crown-like structure, (b) the hydrogen bonding (H-bond) interactions of the ribose part with S102 and S128 coming from alternate monomers, and (c) multiple interactions of the isoalloxazine ring of FMN with the zwitterionic part of I-Tyr, T239, and R104 (Figure 2(b)). The zwitterionic group of I-Tyr is very crucial for its binding in the active site and makes H-bonds with K182, E157, and Y161 of the enzyme.[11] This active site architecture of hIYD is essential for catalytic reductive dehalogenation.

Reductive dehalogenation of iodotyrosine

The reductive deiodination reaction converts I-Tyr to Tyr, forming the FMN_{ox}·hIYD·Tyr state from the FMN_{hq}·hIYD·I−Tyr state. The dynamics in the two end states of the deiodination reaction are distinguished by a larger fluctuation of the α5 helix (residue 167-177) and the α5-α6 loop (residue 178-183) in the FMN_{ox}·hIYD·Tyr state compared to that in the FMN_{hq}·hIYD·I−Tyr state (Figures 3(c) and (d), S7(a)). The H-bond interactions with the side chains of Y161 and E157 weaken drastically in the case of Tyr compared to I-Tyr (Table S4), while the interactions with A130 (of alternate monomer), K182, and R104 remain stable in both systems, while very weak interactions with T238 and T178 are completely lost in the FMN_{ox}·hIYD·Tyr system.

Further active site analysis of FMN_{ox}·hIYD·Tyr shows that H-bond interaction with Y161 side chain oxygen, not only breaks, but the phenolic ring of Y161 undergoes a ring flip (Figure S7(b)). The conformational dynamics of the isoalloxazine ring of flavin provide the actual reason behind this loss of interactions. The average non-covalent interaction (aNCI) analysis reveals a very strong, thermally stable van der Waals interaction between the C-I bond of I-Tyr with the C4a-N5 bond of FMN_{hq} in the FMN_{hq}·hIYD·I−Tyr system (Figure S7(c)). This interaction makes the two bonds parallel to each other maximizing the overlap between them. The free energy profile along the C4-N5-C6 angle and I-C-C4a-N5 dihedral validate the observation quantitatively (Figure S6(b)). FMN_{hq} remains in a puckered conformation in the active site in the FMN_{hq}·hIYD·I−Tyr system. The puckered isoalloxazine ring represents one of the two butterfly modes of FMN_{hq}.[34–37] The van der Waals interaction between I-Tyr and FMN becomes very stable because of this puckering of the isoalloxazine ring with N5 nitrogen coming out of the isoalloxazine plane (Figure 4(a)). Upon deiodination, this van der Waals interaction is lost and the N5 nitrogen comes to the plane of the isoalloxazine ring due to the lack of flexibility of the N1-N10-N5-C6 dihedral (known as the butterfly dihedral) owing to the N-C double bonds between N1-C10a and N5-C4a.

This conformational change of flavin in the FMN_{ox} state becomes associated with a cascading change in the O3′-C3′-C2′-O2′ dihedral of the ribose part of flavin (Figure 4(b)), breaking the very stable H-bond interaction between the 2′-OH of FMN_{ox} and the phenolate group of Tyr (Figure 4(b)). The intramolecular H-bond analysis shows that in the absence of any exter-

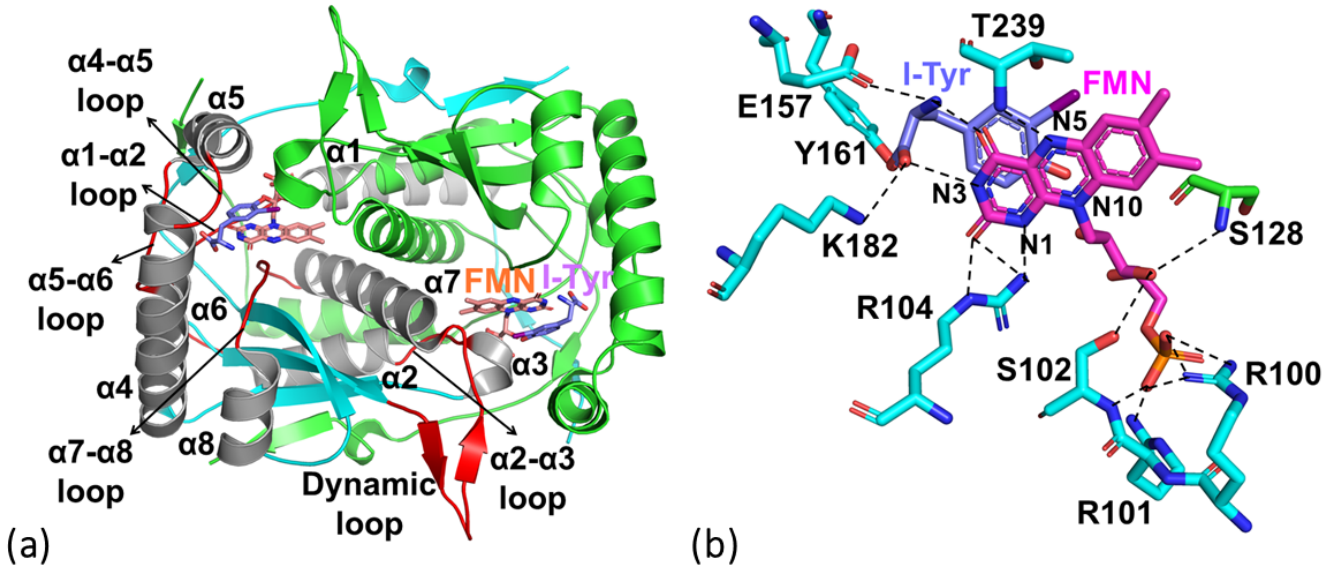

Figure 2: (a) The crystal structure of hIYD in complex with FMN_{hq} and I-Tyr (PDB ID: 4TTC). The helices and loops of monomer A are labelled. (b) The interactions of FMN with I-Tyr and hIYD residues. The residues from monomers A and B are shown in cyan and green color, respectively.

nal molecule (ligand: I-Tyr), the 2′-OH group of flavin forms a very strong H-bond interaction with the N1 nitrogen of the isoalloxazine ring of flavin (a resting state of 2′-OH). Otherwise, the 2′-OH group faces the site of the upcoming molecule to form a recognition H-bond interaction (an active state). This H-bond interaction is essential for substrate recognition by flavin.[38] The loss of 2′-OH H-bond (Figure S7(d) and (e)) with Tyr results in a greater fluctuation (non-hydrogen RMSD) of Tyr as compared to I-Tyr. This further cascades into a loss of H-bond interaction with Y161, T238, and T178.

These three events, i.e., (a) the disappearance of van der Waals interaction between the C-I bond of I-Tyr and the C4a-N5 bond of flavin, (b) the conformational switching of flavin from butterfly mode to planar mode, and (c) the change of the O3′-C3′-C2′-O2′ dihedral of the ribose part of flavin, lead to the weakening and breaking of crucial active site interactions (like Y161 H-bond), causing higher RMSD of ligand in the FMN_{ox}·hIYD·Tyr system. The loss of interactions between ligand and residues of α5-α6 loop leads to the opening of the active site lid helix (α5) indicating a probable product release pathway of Tyr.

Tyrosine release from the active site The end product of the deiodination reaction, Tyr leaves the active site of hIYD with the FMN_{ox} left bound to the enzyme for the next steps of the enzymatic cycle. In the absence of Tyr in the active site, the α4 helix, α4-α5 loop, α5 helix, and α7-α8 loop show higher backbone RMSD in the FMN_{ox}·hIYD state compared to the FMN_{ox}·hIYD·Tyr state (Figures 3(a)-(c), S8(a)). The H-bond interaction analysis demonstrates that A130 (from α3 helix of monomer B), E157 (α4 helix), R104 (α1-α2 loop), K182 (α5-α6 loop) form a stable H-bond network with Tyr in the active site (Table S4). Loss of these interactions in the FMN_{ox}·hIYD state is responsible for the higher RMSD of the corresponding helices and loops. The interactions with K182, E157, and Y161 act as gatekeepers in the catalytic cycle (Figure 5(a)). After the deiodination reaction, the interaction between Tyr and Y161 weakens, causing the Y161 ring to flip, as mentioned earlier. The remaining interactions with K182 and E157 are also lost when Tyr leaves the active site. In the absence of this interaction, the α5 helix opens up like a lid facilitating the release of Tyr to solvent (Figure 5(a))

Our modeled FMN_{ox}·hIYD state is com-

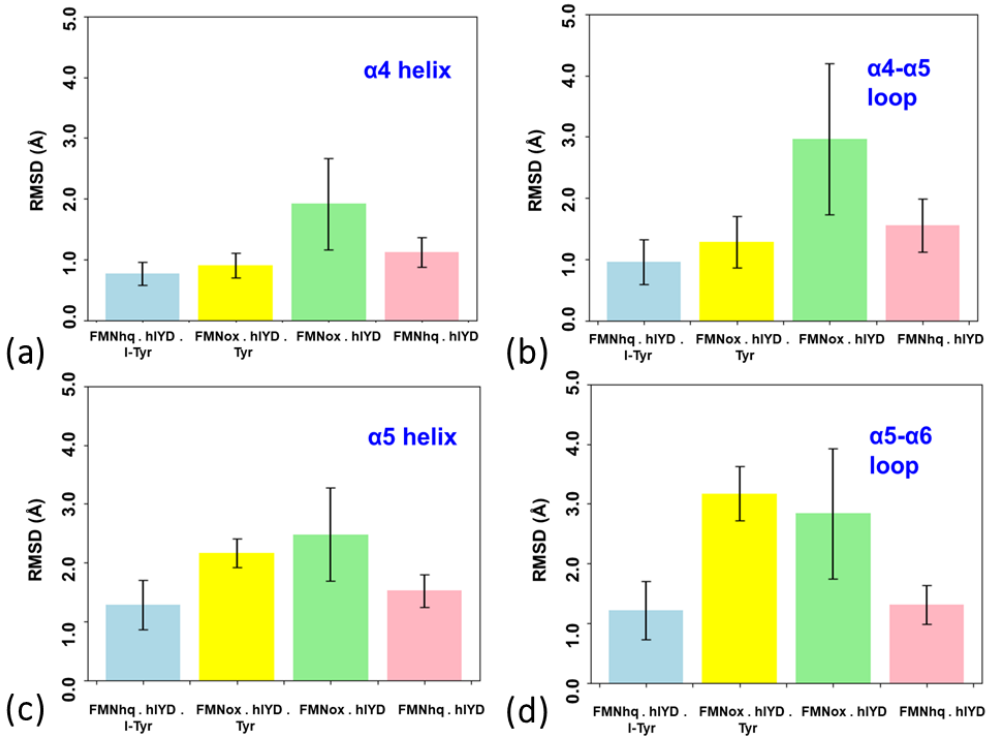

Figure 3: The backbone RMSD of (a) α4 helix, (b) α4-α5 loop, (c) α5 helix, (d) α5-α6 loop in FMN_{hq}·hIYD·I−Tyr, FMN_{ox}·hIYD·Tyr, FMN_{ox}·hIYD, and FMN_{hq}·hIYD systems.

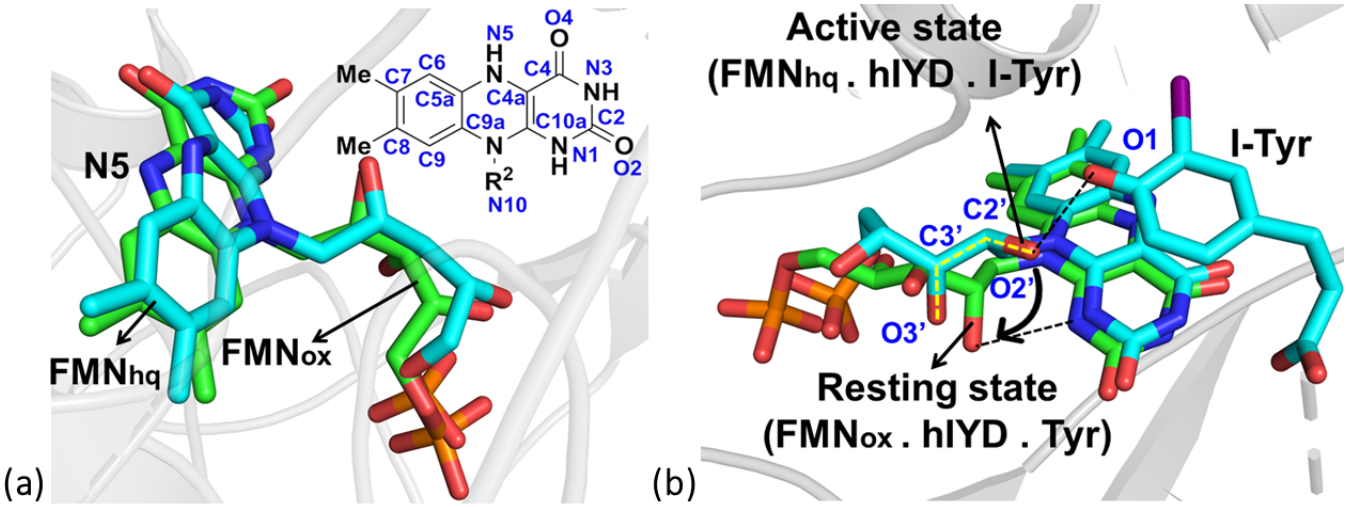

Figure 4: (a) The butterfly mode of the FMN_{hq} ring and the planar mode of the FMN_{ox} in FMN_{hq}·hIYD·I−Tyr and FMN_{ox}·hIYD·Tyr, respectively. The N5 atom of flavin comes out of the isoalloxazine plane in the butterfly mode. The atom numbering of the isoalloxazine ring of flavin is mentioned. (b) The flipping of the O3′-C3′-C2′-O2′ dihedral (yellow dashed line) in FMN_{ox} (green) compared to FMN_{hq} (cyan). The stable H-bond interaction between O1 (phenolate oxygen) of Tyr and 2′-OH of flavin breaks in the FMN_{ox}·hIYD·Tyr system (H-bond interaction is shown by black dotted lines). The active state (in FMN_{hq}·hIYD·I−Tyr system) to resting state (in FMN_{ox}·hIYD·Tyr system) conversion is shown by a black arrow.

parable to the FMN_{ox} bound hIYD (PDB ID: 4TTB) with an average Cα RMSD of 0.8 Å (Figure S8(b)). All the interactions reported in 4TTB crystal structure are present in our modelled FMN_{ox}·hIYD state. In the crystal structure of 4TTB, the electron density of residues 161-178 (end portion of α4 helix, α4-α5 loop, α5 helix) and 199-211 (dynamic loop) are missing. Our simulations shed light on the sequence of events that lead to large conformational dynamics (Figure 5(a)) of hIYD in the FMN_{ox}·hIYD state causing the missing electron density of its residues. Comparison of flavin's interactions shows that the H-bond interactions with S102, R100, R101, R104, T239, and R279 remain consistent in both systems while newly formed H-bonds with K182, A130 (from monomer B) appear in the FMN_{ox}·hIYD state. These interactions explain the lower backbone RMSD of α1-α2 loop and α3 helix in both systems. In both systems, the values of N1-N10-N5-C6 dihedral and C4-N5-C6 angle correspond to the presence of the planar isoalloxazine ring throughout the simulation with a slight increase in planarity in the FMN_{ox}·hIYD state (Figure S6(d) and (e)). This is a result of the loss of the aromatic stacking interaction provided by Tyr to the pyrimidine part of the isoalloxazine ring. However, the conformation of the ribose part of flavin changes largely after the loss of Tyr in the FMN_{ox}·hIYD state (resting state to active state). The new conformation of the 2′-OH group of flavin is essential for the recognition by NADPH in the next step (Figure 5(b)).

NADPH-mediated flavin reduction In the enzymatic cycle of hIYD, NADPH binds to the FMN_{ox}·hIYD state and reduces FMN_{ox} to FMN_{hq}. As mentioned earlier, this step is the most obscure step of the whole enzymatic cycle. The backbone RMSD of α4 helix, α4-α5 loop, α5 helix, and α5-α6 loop become stable in the FMN_{hq}·hIYD system (Figure 3(a)-(d)). The H-bond interactions show that the percentage of H-bonds with S102, R100, R101, R279, T178 and T239 increase in the FMN_{hq}·hIYD state compared to the FMN_{ox}·hIYD state (Table S4) while that with S128 (from monomer B) weakens (Table S4). Our analysis indicates that FMN_{hq} binds more strongly in the active site than FMN_{ox} (ΔG (FMN_{hq}) = −37.3 kcal/mol and ΔG (FMN_{ox}) = −35.3 kcal/mol from MM-PBSA calculations).

T239, a crucial residue in controlling the electron transfer chemistry of flavin, shows a side chain rotation in the FMN_{ox}·hIYD state compared to the FMN_{hq}·hIYD state (Figure 6(a)). T239 provides two H-bond interactions to the N5 of the isoalloxazine ring of flavin via backbone nitrogen and side chain oxygen atoms. The interaction with backbone nitrogen remains stable in both the states (Figure S9(a)), while the side chain oxygen moves to a distance of 5.0 Å when FMN_{ox} is present (Figure 6(a)). The interaction again re-establishes at a distance of 4.0 Å with FMN_{hq} (Figure S9(b)). This agrees with the experimentally observed distances in the crystal structure (PDB ID: 4TTB).[11] The reduction of flavin may have some influence on this phenomenon. The flavin isoalloxazine ring remains stable in its position in both systems as shown by the distance between T239 Cα and the center-of-mass of the isoalloxazine plane (Figure S9(c)). After reduction, the planar isoalloxazine ring again adopts a butterfly mode via puckering of isoalloxazine ring.

In the FMN_{hq}·hIYD state, the 2′-OH flips to a conformation as observed in the FMN_{ox}·hIYD·Tyr state, by the flipping of O3′-C3′-C2′-O2′ dihedral angle (the resting state). Intramolecular H-bond interaction shows that like I-Tyr if NADPH is absent, the 2′-OH group of flavin forms a very strong H-bond interaction with the N1 nitrogen of the isoalloxazine ring of flavin (the resting state of 2′-OH) (Figure 6(b)). The reason behind the presence of an active state in the oxidized form of flavin may be essential for NADPH recognition. However, it will require further experimental and theoretical validation.

Flavin Reactivity We have calculated the local reactivity descriptors (Fukui function) for the FMN_{ox} state in the presence of S102, R100, R104, K182, and T239 side chains to determine the reactive sites in flavin. The compar-

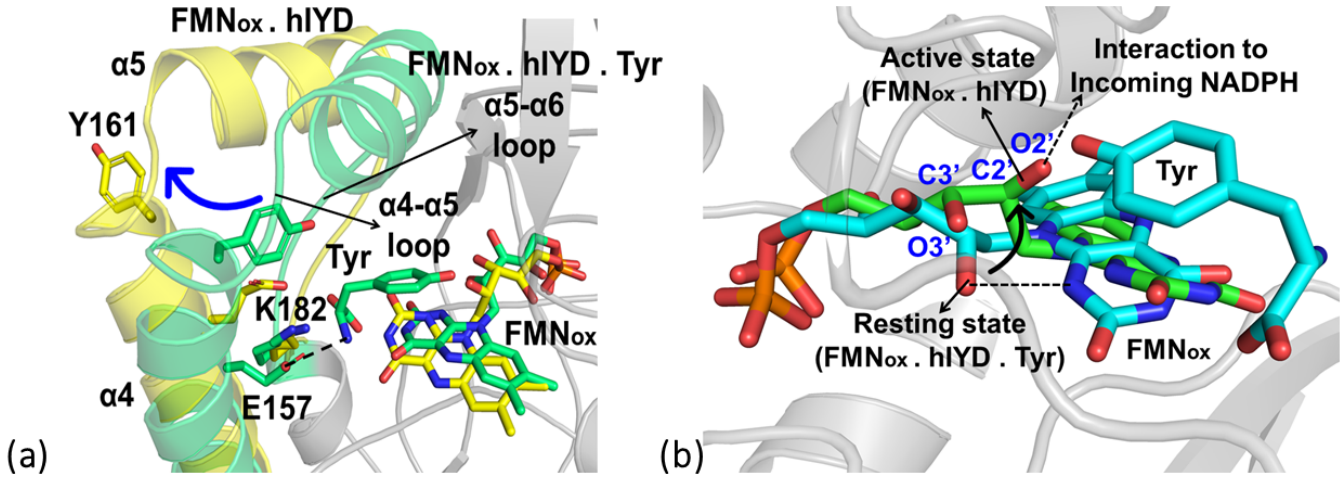

Figure 5: (a) The overlaid conformations of the hIYD in the FMN_{ox}·hIYD·Tyr state (green) and the FMN_{ox}·hIYD state (yellow). Y161, K182, and E157 are shown in green in the FMN_{ox}·hIYD·Tyr state and in yellow in the FMN_{ox}·hIYD state. (b) The 2′-OH group conformation changes from active state (in FMN_{ox}·hIYD, shown in green) to the resting state (in FMN_{ox}·hIYD·Tyr, shown in cyan). The new conformation of the 2′-OH group helps in NADPH recognition.

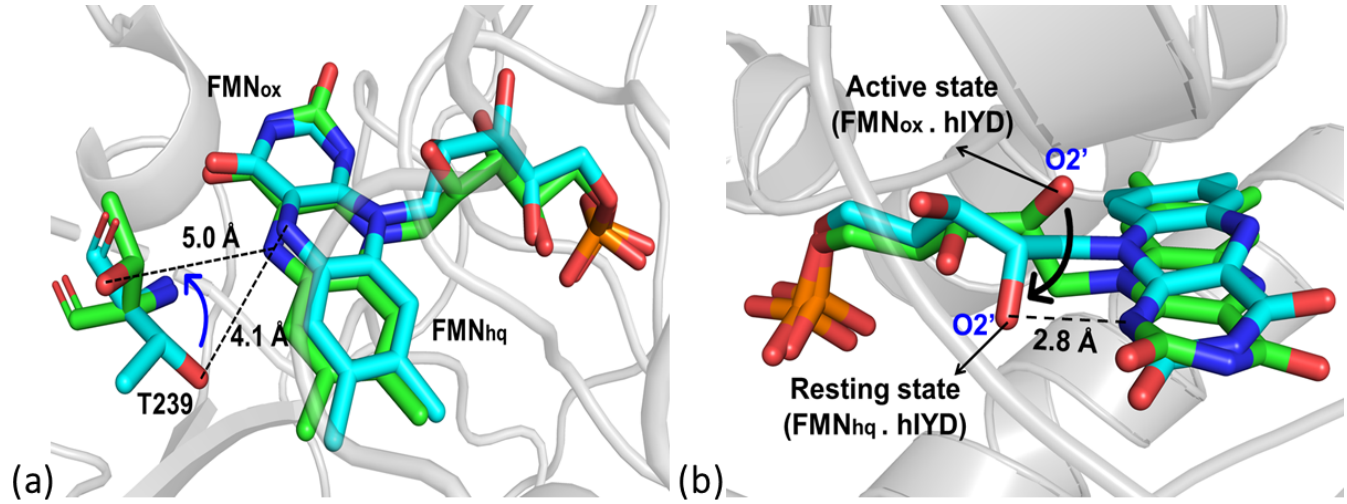

Figure 6: (a) The side chain rotation of T239 in the FMN_{ox}·hIYD state compared to the FMN_{hq}·hIYD state. (b) The active state and resting state of the flavin 2′-OH group in the FMN_{ox}·hIYD and FMN_{hq}·hIYD states.

ison of the FMN_{ox} state in its free form and the presence of enzyme shows a pronounced effect of the enzyme environment in modifying the reactivity sites in FMN_{ox} (Figure S10). The dual descriptors show that N5 nitrogen is the most susceptible center for nucleophilic attack in the presence of the enzyme environment (Table S5 and Figure S10(a) and (b)). This agrees well with the study on 4-hydroxybenzoate hydroxylase which showed that NADPH transfers hydride from C4 to the N5 of FMN_{ox}.[39] Similar results were also found in E. coli nitroreductase NfsA (PDB ID: 1F5V with structural similarity of 16% with hIYD), where C4 of NADPH remained at a 4 Å distance from N5 of flavin for a hydride transfer step.[40] Apart from N5, the C8 carbon also shows an unusually high electrophilic character (Table S5). This is again in good agreement with the fact that the substitution of native FMN by 8-MeO-FMN leads to the formation of a one-electron reduced semiquinone form which is absent for native FMN.[10]

Our results show that the electronic nature of flavin affects its reactivity. To probe the dynamic interaction between NADPH and flavin, we docked NADPH in the active site of hIYD to obtain a model for NADPH-mediated reaction. The best-docked pose showed an extended conformation of NADPH in the active site with C4 of NADPH to N5 of flavin distance of 7.2 Å (Figure S11(a)). In the docking pose, the NADPH forms H-bond interactions with S102, R104, N179, L277, A130 (from alternate monomer), and Y212 (from alternate monomer) (Figure S11(b)). An earlier study has shown that flavin swings out to a position where the enzyme opens up a solvent channel and NADPH remains bound in an extended conformation.[39] To include the dynamic effects, the model system was subjected to a 300 ns MD simulation to check if the interactions found in the docking pose were dynamically stable. During simulation, the conformation of NADPH changes in such a manner that the NADPH C4 and flavin N5 distance comes to a value of 4 Å at around 30 ns. However, this distance keeps fluctuating, and towards the end of the long simulation, the most stable conformation is found to have a C4-N5 distance of 8 Å (Figure 7(a)). The nicotinamide ring of NADPH forms stable H-bond interaction with Y212 from monomer B, and the ribose moiety forms stable H-bond interactions with 2′-OH and 4′-OH group of FMN_{ox}. The residues T178, T273, R279, R104, R100, R101, and S102 provide multiple stable H-bond interactions to the amide, pyrophosphate, and phosphate tail end of the NADPH molecule (Figure 7(b)). These interactions compare well with the previously reported polar interactions.[18,39,40] In vitro, the soluble hIYD, devoid of its N-terminal region loses its sensitivity towards NADPH reduction.[11] The present work shows that in the absence of the N-terminal region, the enzyme can still accommodate NADPH, although the NADPH conformation adopted inside the active site is not suitable for flavin reduction. It is hoped that the interactions observed in the present simulation will serve as a model for further experimental validation.

Iodotyrosine binding in the active site I-Tyr binds in the active site of the FMN_{hq}·hIYD before the reductive deiodination. The enzyme's active site becomes highly organized upon I-Tyr binding (Figure 3(b) and (d)). I-Tyr forms stable H-bond interactions with the 2′-OH group and pyrimidine ring of flavin, Y161, A130 (from alternate monomer), E157, R104, K182, T238, and T178 in the active site (Table S4). These interactions stabilize the α4 helix and α5-α6 loop regions. Consequently, the active site lid (α5 helix) remains in a closed conformation, sequestering the active site from solvent (Figure 8(a)). A comparison of the free energy profiles along the butterfly dihedral N1-N10-N5-C6 and C4-N5-C6 angle shows the effect of I-Tyr binding on the extent of isoalloxazine ring puckering of FMN_{hq} (Figure S6(f) and (c)). The C4-N5-C6 angle remains unchanged, while the N1-N10-N5-C6 dihedral changes to 150° from 135° in the presence of I-Tyr. The presence of I-Tyr establishes stable van der Waals interaction between I-C of I-Tyr and C4a-N5 of flavin (Figure S7(c)), along with aromatic stacking interaction. 2′-

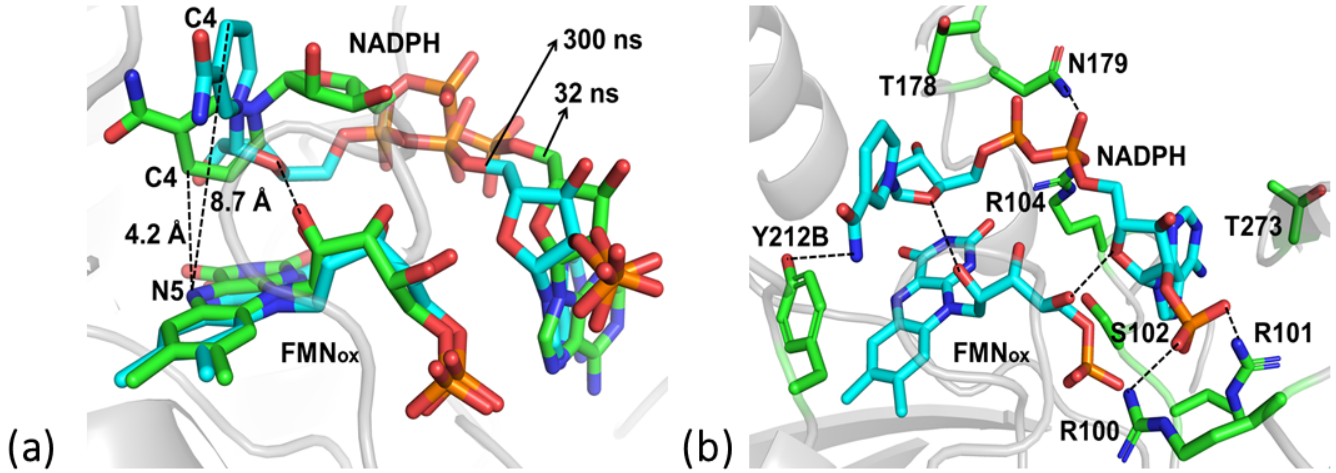

Figure 7: (a) NADPH conformation after 32 ns (green) and 300 ns (cyan) of MD simulation. The initial distance of C4-N5 of 4 Å changes to 8 Å at the end of the simulation. The recognition interaction provided by 2′-OH of flavin is shown. (b) The H-bond interactions between NADPH and the active site residues.

OH changes from the resting state to the active state to reestablish the H-bond interaction with the phenolate group of I-Tyr by (Figure 8(b)). These interactions stabilize the puckered conformation of flavin as necessary for catalysis.

Role of enzyme environment in ligand binding

The electrostatic environment provided by enzyme side chains significantly affects the four steps of the hIYD enzymatic cycle. I-Tyr in the active site is stabilized by strong electrostatic interaction provided by K182, R104, R101, K175, R100, K208 (from alternate monomer), R177, K174, R164, and R279 residues (Figure S12). After reductive dehalogenation, the binding affinity of the product (Tyr) is marginally less than the reactant (I-Tyr), i.e., ΔG (I-Tyr) = −21.1 kcal/mol and ΔG (Tyr) = −14.7 kcal/mol (calculated from MMPBSA method, see Figure 9). Electrostatic interactions provided by R100, K175, and R177 weaken for Tyr, and the interaction with R164 is lost, while a new interaction with R150 forms (Figure S12). On the other hand, flavin is more strongly bound in the active site after deiodination (ΔG (FMN_{hq}) = −39.1 kcal/mol and ΔG (FMN_{ox}) = −42.2 kcal/mol). The FMN_{hq} state is stabilized by electrostatic interactions with R100, R101, R279, R104, K182, K175, R177, K280, K278, and V71 (from alternate monomer) (Figure S12). In the FMN_{ox}-state, flavin makes stronger electrostatic interactions with R279, K278, and K280 (Figure S12). The interaction provided by R177 to FMN_{hq} in FMN_{hq}·hIYD·I−Tyr is replaced by K99 with FMN_{ox} in the FMN_{ox}·hIYD·Tyr system (Figure S12). After Tyr release, the electrostatic interactions of R100, R101, R279, and R104 with FMN_{ox} decrease substantially (Figure S12). This causes lower binding energy of FMN_{ox} state in the FMN_{ox}·hIYD system ΔG (FMN_{ox} in FMN_{ox}·hIYD) = −35.3 kcal/mol as compared to ΔG (FMN_{ox} in FMN_{ox}·hIYD·Tyr) = −42.2 kcal/mol (Figure 9). After NADPH-mediated reduction, the electrostatic interactions of R100, R101, and R279 increase again in the FMN_{hq}·hIYD system leading to higher binding energy of FMN_{hq} state ΔG (FMN_{hq} inFMN_{hq}·hIYD) = −37.3 kcal/mol compared to ΔG (FMN_{ox} in FMN_{ox}·hIYD) = −35.3 kcal/mol (Figure 9). In summary, the basic residues R100, R101, R279, R104, and K182 are crucial for providing flavin stability throughout the catalytic cycle. Therefore, mutation of any of these residues can cause catalytic inactivity of hIYD. This agrees with the genetic studies, where mutations in the DEHAL1 gene (encoding the hIYD enzyme) unravel a connection to

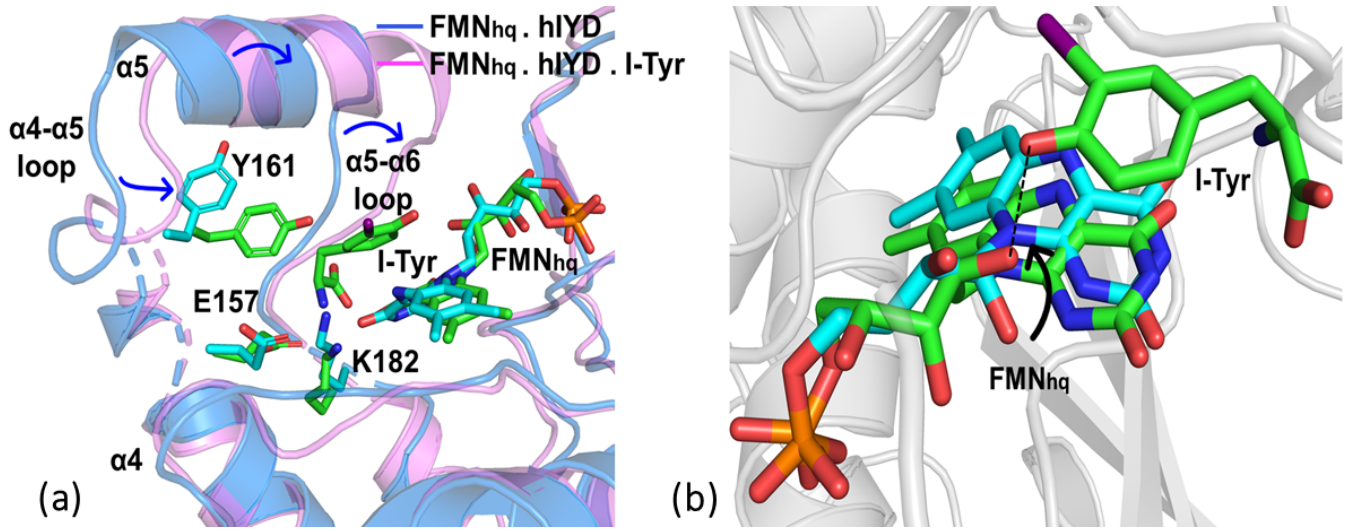

Figure 8: (a) The active site lid closure in hIYD after binding of I-Tyr in the active site. Blue arrows indicate the direction of lid closure. Cyan color residues indicate the FMN_{hq}·hIYD state and green color residues indicate the FMN_{hq}·hIYD·I−Tyr state. (b) The puckered conformation of the flavin ring in the FMN_{hq}·hIYD state (cyan) and the FMN_{hq}·hIYD·I−Tyr state (green). The black dotted line shows the H-bond interaction between the 2′-OH group of flavin and the phenolate group of I-Tyr.

human hypothyroidism.[14,15] The R101F mutation, identified as a cause for hypothyroidism,[14] exposes the delicate balance that these electrostatic interactions maintain. In the absence of R101, the binding of FMN_{hq} state weakens, potentially leading to catalytic inactivity and the diagnosis of hypothyroidism.

Reactivity Trends

The dual reactivity descriptors show that the N5 and N10 atoms of FMN_{hq} are the most susceptible sites for electrophilic attack (Figure S13). The extent of susceptibility increases in the presence of the active site environment (T239 and R104 side chains)(Figure S13). The NBOs contributing to the Fukui functions are localized over the flavin isoalloxazine ring, particularly on N5 and N10 atoms, and C4a-C10a and C7-C8 bonds (Figure S15). The electron density along the C4a-C10a and C7-C8 bonds is due to the resonance of N5 nitrogen's lone pairs via C4a-C10a/C7-C8 double bonds. The HOMO is found to be localized on the isoalloxazine ring π orbital. These results show that the flavin isoalloxazine ring is the powerhouse for reductive dehalogenation in the hIYD en-

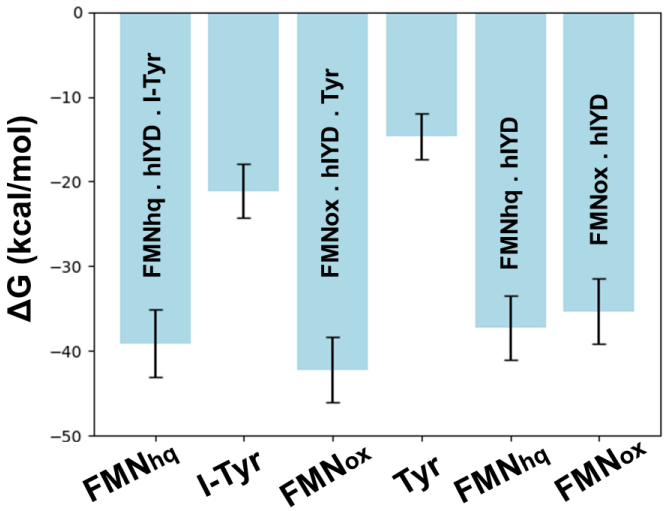

Figure 9: Binding free energy of FMN_{hq}, FMN_{ox} , I-Tyr, and Tyr in FMN_{hq}·hIYD·I−Tyr, FMN_{ox}·hIYD·Tyr, FMN_{ox}·hIYD, and FMN_{hq}·hIYD systems. The error bars are the averaged error of the 10 short trajectories of 10 ns long each.

zyme.

In FMN_{hq}·hIYD·I−Tyr system, the ortho and para carbons of I-Tyr are found more susceptible for electrophilic attack as compared to the N5 and N10 atoms of flavin (Figure S13). This suggests that the first step of IYD catalysis is a proton transfer to the ortho carbon of I-Tyr, as has been earlier suggested by experimental studies.[9,10] The inclusion of the active site residues (T238, R104, and A130B) further enhances the susceptibility without altering the overall pattern of reactivity, revealing the catalytic role of the enzyme (Figure S14). The NBOs contributing to the Fukui functions are located on ortho and para carbons of I-Tyr in phenolate form, which is essential for a successful proton transfer (Figure S15). The HOMO is found to be located on the rings of I-Tyr and flavin. From the nature of the Fukui functions, NBOs, and HOMO, it is clear that the proton transfer step would involve the transfer of an electron from I-Tyr to the σ^* anti-bonding of the bond which will be broken to donate a proton. The σ^* anti-bonding NBO of the N5-H bond of flavin shows a non-zero natural population (Figure S17). Hence, the first proton transfer step is likely to involve the transfer of an electron from I-Tyr to the σ^* anti-bonding of the N-H bond which will be broken to donate a proton.

The phenolate form of I-Tyr is essential for catalysis. This is best illustrated when the reactivity descriptors are compared from the calculations that model I-Tyr in phenolate and phenol forms (Figure S14). When I-Tyr is modeled in phenol form, the most susceptible site for the electrophilic attack in the N5/N10 of flavin, similar to what was seen in FMN_{hq} state without any substrate (Figure S16). In fact, I-Tyr's orthocarbon (attached to iodine) shows susceptibility to nucleophilic attack (Figure S14). In the phenol form of I-Tyr, the HOMO is centered on flavin, as observed in FMN_{hq} state for FMN_{hq}·hIYD system. The distinct change in the reactivity pattern between the phenol and phenolate forms of I-Tyr indicates that the latter form of I-Tyr is essential for the first step of IYD catalysis.

The proton source for the first step of IYD catalysis has remained unanswered. Recent experimental studies showed an inverse correlation between the acidity of N5 proton of flavin and k_{cat} value of I-Tyr dehalogenation and suggested stabilization of the dearomatized intermediate might control the rate of enzymatic dehalogenation.[10] In the present study, we do not find any external source of the proton from our calculations. Even when the active site closes after I-Tyr binding in the FMN_{hq}·hIYD·I−Tyr state, there are no nearby water molecules for proton transfer to the carbon of I-Tyr, as can be seen from the radial distribution function of water (Figure S19). Even the crystal structure does not show any water near (within 5 Å) I-Tyr. Hence, the solvent does not seem to be a proton source. No other residue within 5 Å radius is suitable for proton transfer to the phenolate form of I-Tyr.

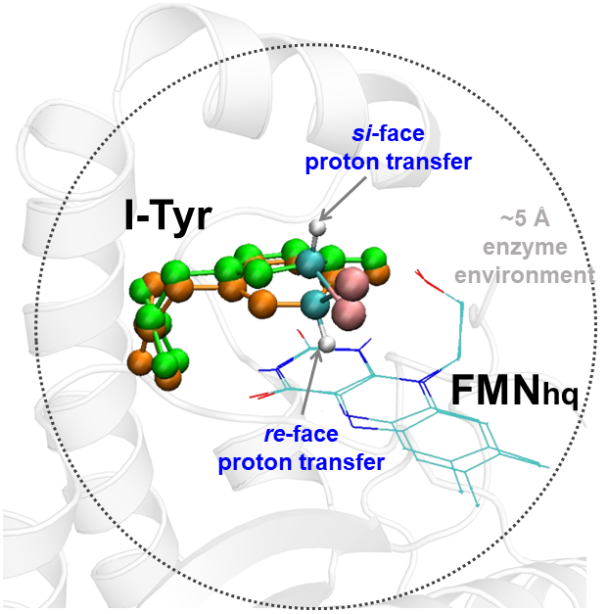

Figure 10: QM cluster optimization of *re*-face and *si*-face proton transfer mechanism in the presence of enzyme environment. The hydrogen atoms, except for the transferred proton, are not shown for clarity. I-Tyr in green shows *si*-face proton transfer and in orange shows *re*-face proton transfer. The I-Tyr ring loses its aromatic stacking when *si*-face proton transfer occurs.

The proton transfer to the orthocarbon can occur from two possible faces: *re*- and *si*-faces. We performed a QM cluster optimization by

taking active sites residues within 5 Å around I-Tyr and FMN_{hq} (with 482 atoms, PM6-D3 method) in the FMN_{hq}·hIYD·I−Tyr system for both *re*-face and *si*-face proton transfer. When the proton approaches from the *si*-face, the prochiral carbon forms an S-chiral centre, and iodine is out of the plane of the phenyl ring by about 1.7 Å facing toward the flavin ring (Figure 10). Such a conformation of the iodine faces a steric clash and interrupts the π stacking interaction between flavin and I-Tyr rings (Figure S18). On the other hand, a proton approaching from the *re*-face not only avoids such a steric clash (Figure 10), but also stabilizes the dearomatized species with non-covalent interaction between I-Tyr and flavin ring (Figure S18). This makes the N5 of FMN, situated 3 Å away from the *re*-face of I-Tyr, the most likely candidate as a proton donor. Although, the experimental studies show that the proton transfer step is not the rate-limiting step in catalysis.[10]

Conclusions

The hIYD enzyme plays a critical role in maintaining the iodine pool of the human body by catalyzing the deiodination of mono- and diiodotyrosines using FMN cofactor. Based on the MD simulations and QM calculations of various stages of hIYD catalysis, we have identified a chain of events in the active site of hIYD that facilitates the catalytic cycle, during which the FMN cofactor adopts alternative conformations using its isoalloxazine ring (planar and butterfly modes) and its ribose group (resting and active state). I-Tyr in the active site of FMN_{hq}·hIYD·I−Tyr is characterized by three unique interactions: a vdW interaction between C-I and the flavin assisted by the butterfly mode of flavin, a hydrogen bond between its phenolate group with the 2′-OH of the ribose group of flavin, and the interaction between its zwitterionic group with the gatekeeper residues like K182, E157, and Y161. Upon reductive deiodination of I-Tyr, the flavin adopts a planar conformation triggering the ribose to adopt the resting state where Tyr loses its hydrogen bond with the ribose 2′-OH group, leading to a greater fluctuation of Tyr that further escalates to loss of interaction with the gatekeeper residues, thus opening the active site lid helix (α5) for efficient Tyr release. After Tyr release, the ribose group regenerates the active state of 2′-OH that serves as the crucial site for NADPH recognition. The favorable conformation of NADPH with a small distance between its C4 and flavin's N5, accompanied by a high nucleophilicity of N5 of FMN_{ox} makes FMN_{ox} reduction facile. The enzyme employs basic residues like R100, R101, R279, R104, and K182 with S102 to stabilize the flavin cofactor throughout the catalytic cycle, indicating a list of potential mutations that can have a crucial effect on iodine regulation in the human body. In the absence of any indication of an external source of proton and based on the electronic and conformational analysis, N5 nitrogen of flavin is the likely proton source from the *re*-face of the C-I bond of I-Tyr during the first proton transfer step.

Asscociated content

Supporting Information The Supporting Information is available with additional tables, figures, and methodological details.

Author information

Corresponding Author
Sabyashachi Mishra - Department of Chemistry, Indian Institute of Technology, Kharagpur - 721302, India. https://orcid.org/0000-0002-2551-1021 Email: mishra@chem.iitkgp.ac.in
Authors
Soumyajit Karmakar - Department of Chemistry, Indian Institute of Technology, Kharagpur - 721302, India. https://orcid.org/0000-0003-4867-0970

Declaration of competing interest

The authors declare that they have no conflicts of interest in the contents of this article.

Acknowledgement SK acknowledges the Prime Minister's Research Fellowship, the Ministry of Education, Government of India for support. The authors thank Prof. Samik Nanda and Mr. Sourav Manna for useful discussion. SM acknowledges the support from SERB, DST, Govt. of India (CRG/2022/004088 and SR/FST/CSII-026/2013). This work used the resources of the Paramshakti supercomputing facility of IIT Kharagpur, established under the National Supercomputing Mission of the Government of India and supported by CDAC, Pune.

References

(1) Song, K.; Wang, Y.; Wang, Y.; Yao, W.; Tang, Y.; Tian, X.; Song, X.; Zhou, J. Advances in Thyroid Organoids Research and Applications. *Endocr. Res.* **2024**, 1–6.

(2) Zbigniew, S. Role of iodine in metabolism. *Recent Pat. Endocr. Metab. Immune Drug Discov.* **2016**, *10*, 123–126.

(3) Schomburg, L.; Köhrle, J. On the importance of selenium and iodine metabolism for thyroid hormone biosynthesis and human health. *Mol. Nutr. Food Res.* **2008**, *52*, 1235–1246.

(4) Sorrenti, S.; Baldini, E.; Pironi, D.; Lauro, A.; D'Orazi, V.; Tartaglia, F.; Tripodi, D.; Lori, E.; Gagliardi, F.; Praticò, M.; others Iodine: Its role in thyroid hormone biosynthesis and beyond. *Nutrients* **2021**, *13*, 4469.

(5) Sun, Z.; Su, Q.; Rokita, S. E. The distribution and mechanism of iodotyrosine deiodinase defied expectations. *Arch. Biochem. Biophys.* **2017**, *632*, 77–87.

(6) Köhrle, J.; Frädrich, C. Deiodinases control local cellular and systemic thyroid hormone availability. *Free Radic. Biol. Med.* **2022**,

(7) Querido, A.; Stanbury, J. B.; Kassenaar, A.; Meijer, J. The metabolism of iodotyrosines. III. Di-iodotyrosine deshalogenating activity of human thyroid tissue. *J. Clin. Endocrinol. Metab.* **1956**, *16*, 1096–1101.

(8) Rokita, S. E.; Adler, J. M.; McTamney, P. M.; Watson Jr, J. A. Efficient use and recycling of the micronutrient iodide in mammals. *Biochimie* **2010**, *92*, 1227–1235.

(9) Bobyk, K. D.; Ballou, D. P.; Rokita, S. E. Rapid kinetics of dehalogenation promoted by iodotyrosine deiodinase from human thyroid. *Biochemistry* **2015**, *54*, 4487–4494.

(10) Kozyryev, A.; Lemen, D.; Dunn, J.; Rokita, S. E. Substrate Electronics Dominate the Rate of Reductive Dehalogenation Promoted by the Flavin-Dependent Iodotyrosine Deiodinase. *Biochemistry* **2023**, *62*, 1298–1306.

(11) Hu, J.; Chuenchor, W.; Rokita, S. E. A switch between one-and two-electron chemistry of the human flavoprotein iodotyrosine deiodinase is controlled by substrate. *J. Biol. Chem.* **2015**, *290*, 590–600.

(12) Mondal, S.; Manna, D.; Raja, K.; Mugesh, G. Halogen bonding in biomimetic deiodination of thyroid hormones and their metabolites and dehalogenation of halogenated nucleosides. *ChemBioChem* **2020**, *21*, 911–923.

(13) Mondal, S.; Raja, K.; Schweizer, U.; Mugesh, G. Chemistry and biology in the biosynthesis and action of thyroid hormones. *Angew. Chem. Int. Ed.* **2016**, *55*, 7606–7630.

(14) Moreno, J. C.; Klootwijk, W.; van Toor, H.; Pinto, G.; D'Alessandro, M.; Lèger, A.; Goudie, D.; Polak, M.; Grüters, A.; Visser, T. J. Mutations in the iodotyrosine deiodinase gene and hypothyroidism. *New Eng. J. Med* **2008**, *358*, 1811–1818.

(15) Moreno, J. C.; Visser, T. J. Genetics and phenomics of hypothyroidism and goiter due to iodotyrosine deiodinase (DEHAL1) gene mutations. *Mol. Cell. Endocrinol.* **2010**, *322*, 91–98.

(16) Sun, Z.; Rokita, S. E. Toward a halophenol dehalogenase from iodotyrosine deiodinase via computational design. *ACS Catal.* **2018**, *8*, 11783–11793.

(17) Watson Jr, J. A.; McTamney, P. M.; Adler, J. M.; Rokita, S. E. Flavoprotein iodotyrosine deiodinase functions without cysteine residues. *ChemBioChem* **2008**, *9*, 504–506.

(18) Taga, M. E.; Larsen, N. A.; Howard-Jones, A. R.; Walsh, C. T.; Walker, G. C. BluB cannibalizes flavin to form the lower ligand of vitamin B12. *Nature* **2007**, *446*, 449–453.

(19) Gordon, J. C.; Myers, J. B.; Folta, T.; Shoja, V.; Heath, L. S.; Onufriev, A. H++: a server for estimating p K as and adding missing hydrogens to macromolecules. *Nucleic Acids Res.* **2005**, *33*, W368–W371.

(20) Maier, J. A.; Martinez, C.; Kasavajhala, K.; Wickstrom, L.; Hauser, K. E.; Simmerling, C. ff14SB: improving the accuracy of protein side chain and backbone parameters from ff99SB. *J. Chem. Theory Comput.* **2015**, *11*, 3696–3713.
(21) Bayly, C. I.; Cieplak, P.; Cornell, W.; Kollman, P. A. A well-behaved electrostatic potential based method using charge restraints for deriving atomic charges: the RESP model. *J. Phys. Chem.* **1993**, *97*, 10269–10280.
(22) Wang, J.; Wolf, R. M.; Caldwell, J. W.; Kollman, P. A.; Case, D. A. Development and testing of a general amber force field. *J. Comput. Chem.* **2004**, *25*, 1157–1174.
(23) Mark, P.; Nilsson, L. Structure and dynamics of the TIP3P, SPC, and SPC/E water models at 298 K. *J. Phys. Chem. A* **2001**, *105*, 9954–9960.
(24) Case, D.; Ben-Shalom, I.; Brozell, S.; Cerutti, D.; Cheatham III, T.; Cruzeiro, V.; Darden, T.; Duke, R.; Ghoreishi, D.; Gilson, M.; others AMBER 2018; 2018. *University of California, San Francisco* **2018**,
(25) Elber, R.; Ruymgaart, A. P.; Hess, B. SHAKE parallelization. *Eur Phys J Spec Top* **2011**, *200*, 211–223.
(26) Isele-Holder, R. E.; Mitchell, W.; Ismail, A. E. Development and application of a particle-particle particle-mesh Ewald method for dispersion interactions. *J. Chem. Phys.* **2012**, *137*.
(27) Davidchack, R. L.; Handel, R.; Tretyakov, M. Langevin thermostat for rigid body dynamics. *J. Chem. Phys.* **2009**, *130*.
(28) Berendsen, H. J.; Postma, J. v.; Van Gunsteren, W. F.; DiNola, A.; Haak, J. R. Molecular dynamics with coupling to an external bath. *J. Chem. Phys.* **1984**, *81*, 3684–3690.
(29) Roe, D. R.; Cheatham III, T. E. PTRAJ and CPPTRAJ: software for processing and analysis of molecular dynamics trajectory data. *J. Chem. Theory Comput.* **2013**, *9*, 3084–3095.
(30) Massova, I.; Kollman, P. A. Combined molecular mechanical and continuum solvent approach (MM-PBSA/GBSA) to predict ligand binding. *Perspect. Drug Discov. Des.* **2000**, *18*, 113–135.
(31) Miller III, B. R.; McGee Jr, T. D.; Swails, J. M.; Homeyer, N.; Gohlke, H.; Roitberg, A. E. MMPBSA. py: an efficient program for end-state free energy calculations. *J. Chem. Theory Comput.* **2012**, *8*, 3314–3321.
(32) Frisch, M. J. et al. Gaussian˜16 Revision C.01. 2016; Gaussian Inc. Wallingford CT.
(33) Lu, T.; Chen, F. Multiwfn: A multifunctional wavefunction analyzer. *J. Comput. Chem.* **2012**, *33*, 580–592.
(34) Kabir, M. P.; Orozco-Gonzalez, Y.; Gozem, S. Electronic spectra of flavin in different redox and protonation states: a computational perspective on the effect of the electrostatic environment. *Phys. Chem. Chem. Phys.* **2019**, *21*, 16526–16537.
(35) Nakai, S.; Yoneda, F.; Yamabe, T. Theoretical study on the lowest-frequency mode of the flavin ring. *Theor. Chem. Acc.* **1999**, *103*, 109–116.
(36) Kar, R. K.; Miller, A.-F.; Mroginski, M.-A. Understanding flavin electronic structure and spectra. *Wiley Interdiscip. Rev. Comput. Mol. Sci.* **2022**, *12*, e1541.
(37) Aleksandrov, A. A molecular mechanics model for flavins. *J. Comput. Chem.* **2019**, *40*, 2834–2842.
(38) Luo, M.; Arentson, B. W.; Srivastava, D.; Becker, D. F.; Tanner, J. J. Crystal structures and kinetics of monofunctional proline dehydrogenase provide insight into substrate recognition and conformational changes associated with flavin reduction and product release. *Biochemistry* **2012**, *51*, 10099–10108.
(39) Wang, J.; Ortiz-Maldonado, M.; Entsch, B.; Massey, V.; Ballou, D.; Gatti, D. L. Protein and ligand dynamics in 4-hydroxybenzoate hydroxylase. *Proc. Natl. Acad. Sci. U.S.A.* **2002**, *99*, 608–613.
(40) White, S. A.; Christofferson, A. J.; Grainger, A. I.; Day, M. A.; Jarrom, D.; Graziano, A. E.; Searle, P. F.; Hyde, E. I. The 3D-structure, kinetics and dynamics of the E. coli nitroreductase NfsA with NADP+ provide glimpses of its catalytic mechanism. *FEBS Lett.* **2022**, *596*, 2425–2440.

TOC Graphic